Chapter 8
Remote Sensing Studies on Monitoring Natural Hazards Over Cultural Heritage Sites in Cyprus

Athos Agapiou and Vasiliki Lysandrou

Abstract This chapter presents examples of remote sensing studies for monitoring natural hazards related to ancient monuments and archaeological sites in Cyprus. Through these studies, the use of Earth Observation, and specifically the contribution of the European Copernicus Programme, is highlighted. Most of them have been carried out during the last years, within the framework of funded research projects. The various case studies presented in this chapter underscore Earth Observation's mingling with other remote sensing techniques (both middle range and terrestrial) and geoinformatics towards inclusive monitoring of cultural heritage and prevention against possible hazards.

The chapter unfolds in two parts: The first part introduces an overview of the potential contribution of Earth Observation to the Cultural Heritage Disaster Risk Management (DRM) cycle, with specific focus on the Eastern Mediterranean basin. The DRM includes six consecutive steps that require various inputs, including the context, threats and monitoring phases. For each step, the role of Earth Observation sensors and their related products are discussed.

The second part of this chapter focuses on studies dealing with natural hazards in Cyprus using optical and radar datasets. These studies include the following: (a) soil erosion by water, (b) vegetation growth, and (c) detection of surface displacements, in sites with archaeological interest.

The chapter ends with a comprehensive risk assessment report of various hazards (both natural and anthropogenic) using the Analytical Hierarchy Process (AHP) method. This assessment concerns the western part of Cyprus, namely the Paphos District, where more than 200 monuments are found.

A. Agapiou (✉) · V. Lysandrou
Department of Civil Engineering & Geomatics, Cyprus University of Technology, Limassol, Cyprus

Eratosthenes Centre of Excellence, Limassol, Cyprus
e-mail: athos.agapiou@cut.ac.cy; vasiliki.lysandrou@cut.ac.cy

167

8.1 Introduction

This chapter aims to present various authors' studies performed in the last years, through research activities, dealing with natural hazards over cultural heritage sites. The chapter has a specific focus on the Eastern Mediterranean basin and Cyprus, as well as remote sensing data, and Earth Observation sensors. At the beginning of the chapter, an overview of the potential contribution of Earth Observation to the Cultural Heritage Disaster Risk Management (DRM) cycle is presented. The DRM cycle and the role of the Earth Observation sensors are emphasised in the next section. The synthesis and assessment from various hazards (both natural and anthropogenic) using the Analytical Hierarchy Process (AHP) methodology are then presented.

Hazards can have a negative impact on cultural heritage, while a combination of hazards may trigger other secondary ones. As identified by International Council for Science (ICSU) and the World Meteorological Organization (WMO), and adopted by UNESCO, the most common categories of hazards are the following: meteorological, hydrological, geological, astrophysical, biological, and climate change (UNESCO, 2010).

In the literature, various terms have been used to study the hazards' phenomena. *Disaster* is defined by the United Nations International Strategy for Disaster Reduction as "a severe disruption of the functioning of a community or a society causing widespread human, material, economic or environmental losses which exceeds the ability of the affected community or society to cope using its resources" (United Nations, 2009). This definition was extended by other international organisations, dealing with the management of cultural heritage sites, in order to include disaster impacts not only on people and properties but also on the cultural heritage values of the World Heritage property (UNESCO, 2010).

Risk is defined as "the chance of something happening that will have an impact upon objectives" (Emergency Management Australia, 2000), while the United Nations (2009) refers to *risk* as to the combination of the probability of an event and its negative consequences. Moreover, *hazard* is defined as "a dangerous phenomenon, substance, human activity or condition that may cause loss of life, injury or other health impacts, property damage, loss of livelihoods and services, social and economic disruption, or environmental damage or any phenomenon, substance or situation" (United Nations, 2009). Hazard can eventually cause disruption or damage to different infrastructures and services, people, property, and environment (Abarquez and Murshed, 2004). Finally, *vulnerability* refers to "the characteristics and circumstances of a community, system or asset that make it susceptible to the damaging effects of a hazard" (United Nations, 2009). Based on these terms, vulnerability is an intrinsic characteristic of an asset, independent of its exposure. Consequently, *disaster risk* is described as the result of hazard and vulnerability (UNESCO, 2010).

Earth Observation plays an essential role in monitoring cultural heritage sites' purposes against various anthropogenic or natural hazards. The existing literature
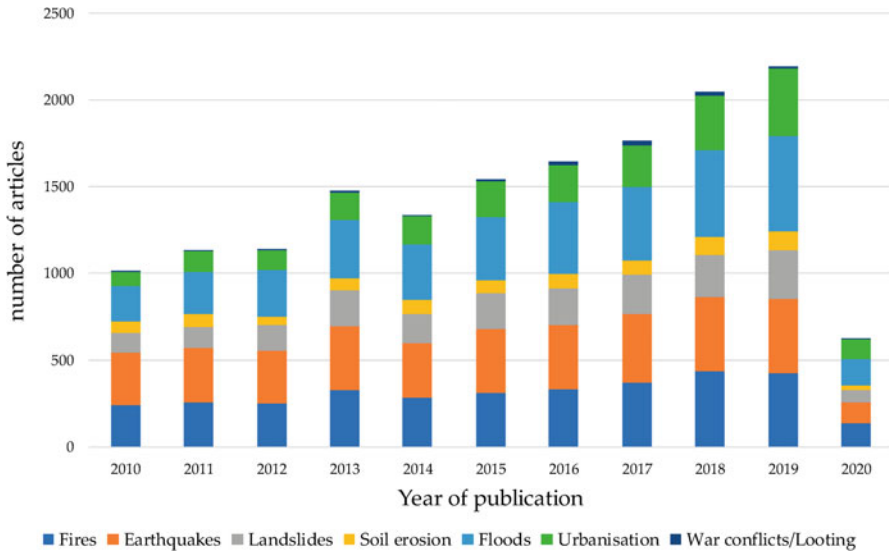
Fig. 8.1 The total number of published articles related to various hazards with the support of satellite and space-based observations for the last decade (2010–2020). (Source: Agapiou et al., 2020b)

indicates a steady increase in scientific studies dealing with this topic (Fig. 8.1). This is mainly due to satellite sensors' advantages, such as performing systematic measurements remotely covering large areas. The increasing number of new sensors has also released new opportunities to support cultural heritage sites' systematic monitoring. For instance, the European Copernicus Sentinel-2 constellation provides optical images with a revisit time of 5 days at the equator, while these data are freely distributed and open access (Li & Roy, 2017). Other initiatives and services like the Copernicus Emergency Management Services, (Bosco et al., 2021), the International Charter Space and Major Disasters (2021), the United Nations Platform for Space-based Information for Disaster Management and Emergency Response (UN-SPIDER) (2021) or Group on Earth Observation (GEO) (2021), can provide support to local authorities after significant disastrous situations.

8.2 Disaster Risk Management (DRM) Cycle and Earth Observation Contribution

The Disaster Risk Management (DRM) cycle proposed by the International Strategy for Disaster Reduction and other international organisations and committees (Unesco, 2010, ICCROM 2016, ISO 31000, 2018) comprises six steps, briefly outlined below. All steps are interlinked between them, and hence any assumptions and ambiguities impact the full implementation of the DRM cycle. The design and

conceptualisation of a DRM cycle plan is a synergistic effort of several qualified parties to obtain specific local value information.

Disaster Risk Management (DRM) Cycle Steps *Step I*: Understanding the context; *Step II*: Identifying risks; *Step III*: Analysing risks; *Step IV*: Evaluating risks; *Step V*: Treating risks; *Step VI*: Monitoring phase.

The first step includes collecting relevant information about various aspects of a cultural heritage site. The information can include details related to the physical environment and administrative, legal, political, socio-cultural, and economic aspects of a site. Ste II of the DRM cycle comprises identifying relevant natural and human-made risks that can potentially threaten cultural heritage. Then, at step III, the possibility of a threat is calculated, and the expected impact of all risks is estimated. Then, at step IV, the hierarchy and the classification of all potential risks is performed. At the following step, relevant effective measures can be planned by local stakeholders to eliminate or minimise the negative impact of the identified risks. Finally, the monitoring phase, includes a periodic update of all information

Following this brief introduction regarding the DRM cycle, a recent study (Agapiou et al., 2020b) attempted to link these steps of the DRM cycle with Earth Observation potentials. Therefore, for each step, likely synergies between Earth Observation sensors' existing capacity and cultural heritage management needs were investigated.

Regarding step I (context) and step II (identification of risks), remotely sensed sensors might be used for documentation and cartographic purposes. Diachronic observations over the site can be achieved through satellite and aerial observations providing time-series land use maps. This can support a better understanding of the archaeological site's potential changes. Beyond the existing high-resolution satellite multispectral sensors, archival satellite and aerial datasets can be used to map landscapes before modern development and changes (Hritz, 2013; Agapiou et al., 2016a; Ur, 2016; Lysandrou and Agapiou, 2020; Casana, 2020). Other existing geo-datasets like risk maps for geohazards and maps produced after processing satellite-based information (such as geo-datasets related to soil erosion by water) are available for Europe through specific platforms (Panagos et al., 2012).

Step III, concerns the risk assessment/risk analysis, which can be achieved from satellite images and related products, as can be seen in Solari et al., 2020; Tapete et al., 2016; Pastonchi et al., 2018, for floods, landslides, looting etc. Based on all previous steps, the overall risk is estimated in step IV. During step V, actions to prevent and/or limit the identified risks' overall damage occur. Here the role of Earth Observation sensors can be supportive for cases like illegal actions over archaeological sites. Even though satellite-based observations cannot prevent illegal actions on the ground, identifying looted areas can be considered a critical step towards increasing awareness for potential illegal trafficking and the protection of cultural assets.

Fig. 8.2 Favourable characteristics of satellite observation datasets for cultural heritage's DRM. (After Agapiou et al., 2020b)

Finally, at step VI, the role of remotely sensed data can be fundamental for systematic monitoring of archaeological sites. The spatial extent of satellite images and the continuous observation over archaeological sites can be easily achieved using remote sensing techniques. For instance, the Copernicus satellite sensors' high temporal revisiting time (5-days) is ideal for the systematic observation since they can continuously provide new data, even of areas that are not physically accessible. Figure 8.2 summarises the primary characteristics of satellite sensors, which can support DRM cycles.

Therefore, the role of satellite observations and connected remotely sensed sensors are multiple. Examples from this role can be seen in Fig. 8.3. Despite that the list is not exhaustive, it indicates satellite observations' potentials toward implementing the DRM cycle.

8.3 Examples of Remote Sensing Studies for Monitoring Natural Hazards Over Cultural Heritage Sites in Cyprus

In this section, various studies regarding natural hazards over heritage sites in Cyprus using Earth Observation and other remotely sensed data are presented. Natural hazards include the impact of soil erosion by water, vegetation growth and dynamics, and the detection of surface displacements.

8.3.1 Soil Erosion

Soil erosion by water is a natural phenomenon that involves the detachment of soil material rainfall and the flow traction (Erosion by Water, 2021). Models regarding
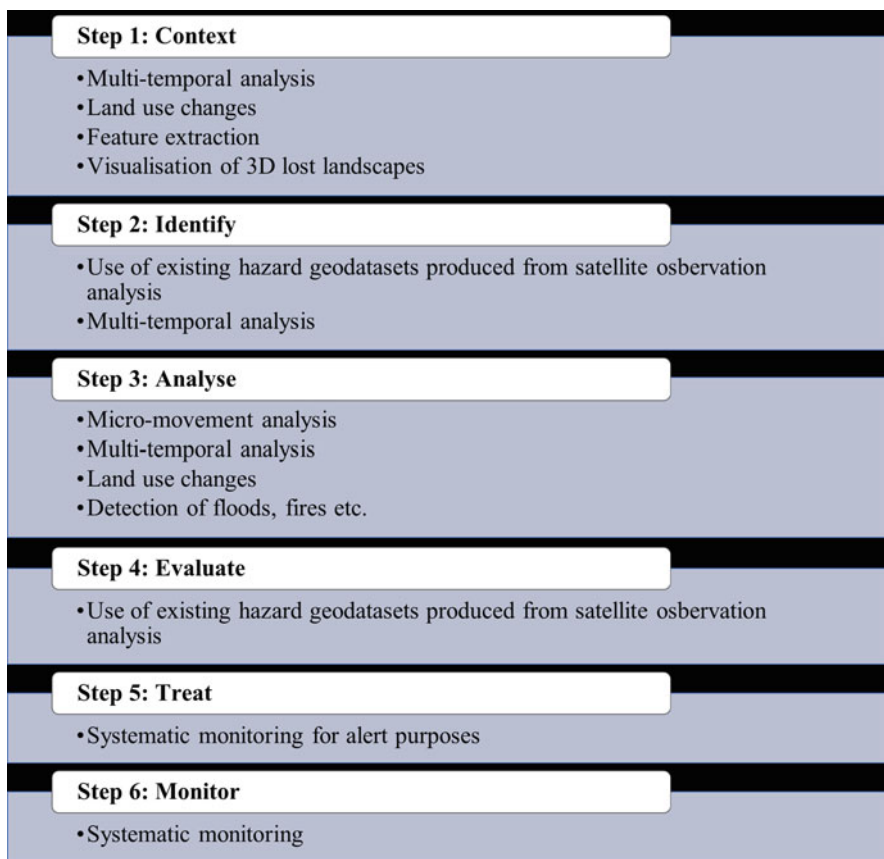
Fig. 8.3 Indicative key satellite observation processing chains beneficial for the various steps of a DRM cycle intended for cultural heritage. (After Agapiou et al., 2020b)

the study of soil erosion have been investigated in the past by Panagos (2015), Panagos and Katsoyannis (2019), Pena et al. (2020) and Chandramohan et al. (2015); for more related literature, see Agapiou et al. (2020a).

These studies have used various models to better estimate and predict soil loss (Quinton, 2011). The use of empirical models like the Revised Universal Soil Loss Equation (RUSLE) has been widely used due to reasonably accurate estimations and its capacity to be implemented, using a Geographical Information System (GIS) and satellite datasets (Borrelli et al., 2013). RUSLE model, developed by Renard et al. (1997), uses five factors: multiplying each other. These factors are the rainfall erosivity factor (R), the soil erodibility factor (K), the slope length and steepness factor (LS), the cover management factor (C), and the conservation practice factor (P) for the estimation of the average annual soil loss (A) (for a review regarding this model see Ghosal and Das Bhattacharya, 2020). Through the Panagos et al. (2012) study, RUSLE datasets have become accessible on a European level. European and

global soil erosion maps and geodata sets, like those of Panagos et al. (2012), can be accessed by the European Soil Data Centre (ESDAC).

Soil erosion by water remains one of the most important natural hazards that are threatening archaeological sites. Both soil loss and soil deposition can alter an area's archaeological context, transferring, for instance, ceramics from one location to another. Archaeological context includes not only the standing monuments but also subsurface archaeological remains. For the lastest, our knowledge is limited for several sites, making their protection very difficult. While some heritage management methods using ground-based strategies have been reported in the past (see Luo et al., 2019), these have a limited spatial extent. Therefore, evaluating the risk of subsurface archaeological remains from soil erosion over large areas is peculiarly difficult. In a recent article, Agapiou et al. (2020a) used Kibblewhite et al. (2015) datasets to develop a sub-surface archaeological proxy map at a European level. In their work, Kibblewhite et al. (2015) have categorised European soil according to how the various archaeological materials can be affected by the pertinent soil type, following a standard taxonomic classification. The study from Agapiou et al. (2020a) has integrated these datasets to provide for the first European estimation of subsurface archaeological exposure due to soil loss. Simultaneously, the results are biased on the models' uncertainty and assumptions and the datasets used—the analysis aimed to pave the way to implement extensive-scale studies related to subsurface archaeological materials threats. The overall results are shown in Fig. 8.4. The analysis indicated that 75% of the area is characterised as a low threat due to soil erosion, with soil loss of less than 5 t/ha per year. In comparison, 13% and 12% are characterised with moderate (soil loss between 5–10 t/ha per year) and high-risk (soil loss more than 10 t/ha per year) level.

In detail, as shown from Fig. 8.4, four different subsurface materials, namely the metals, bones, organics, and stratigraphy evidence, have been investigated against soil loss. The preservation state of each type of stratigraphic material is mapped as poor (red), fair (yellow), and good (green). Areas with no data available are visualised with white colour in the background. The majority of the area for all types of archaeological material is considered low-threat regardless of their soils' preservation capacity. However, regarding the moderate- and high-threat level areas, fluctuations can be observed. South Europe, including the case study of Cyprus and the Mediterranean basin, is exposed to higher soil-loss threats compared to northern countries. A country-level statistic based on the findings of Fig. 8.4 was also implemented. These are shown in Figs. 8.5, 8.6, 8.7 and 8.8. Figure 8.5 indicates the mean values per country level for metals concerning the level of soil-loss threats, while Figs. 8.6, 8.7 and 8.8 indicate the same results for bones, organics, and stratigraphic evidence, respectively. For all Figs. 8.5, 8.6, 8.7 and 8.8, values close to 1 indicate the low preservation status, values close to 2 indicate fair conditions of preservation, and values close to 3 good preservation status.

The primary outcomes of the previous study were the following: (1) Most European countries can be considered low threat areas for all types of subsurface materials; (2) Northern European countries can be considered low threat areas in contrast to Mediterranean countries, which are characterised with moderate and
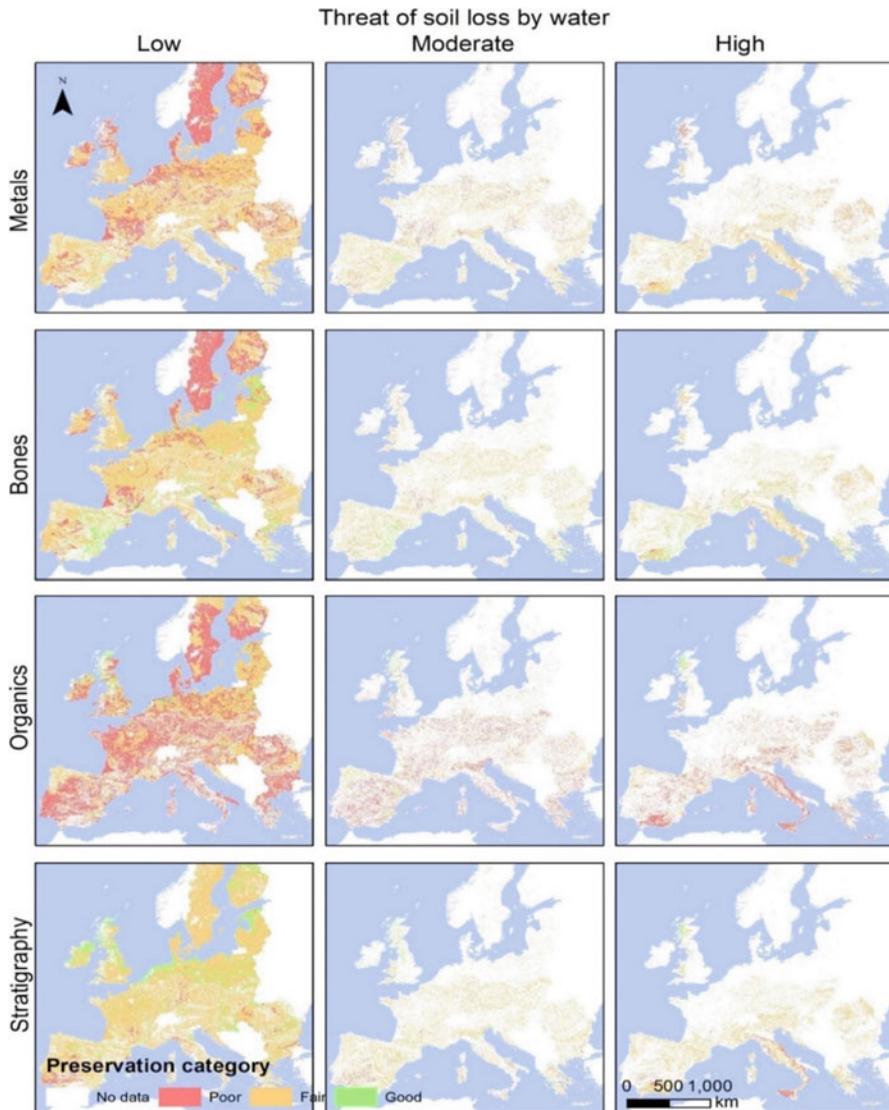
Fig. 8.4 Maps indicating the level of threat (low, moderate, and high) based on soil loss provoked by water activity (soil erosion) for each of the four different subsurface materials (metals, bones, organics, and stratigraphy evidence): The preservation state is also indicated (red for poor, yellow for fair, and green for good). (Source: Agapiou et al., 2020a)

high-risk levels; (3) Areas characterised as low threat from soil erosion present approximately 10% of adequate preservation capacity, which varies depending on the type of the material; (4) Similar patterns on a European scale for all types of materials are reported for areas characterised with moderate and high risk from soil loss.
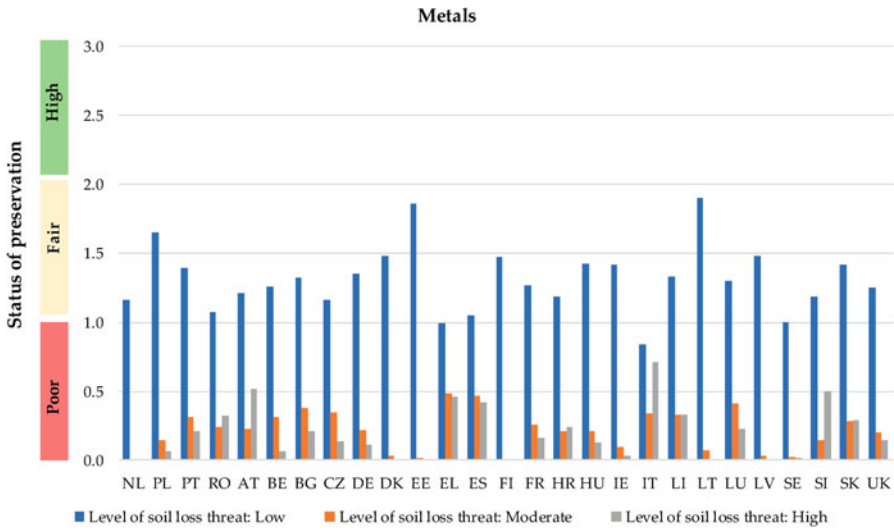
Fig. 8.5 Mean values per country level for metals per level of soil-loss threats: Values close to 1 indicate the poor preservation status, values close to 2 indicate fair conditions of preservation, and values close to 3 good preservation status. (Source: Agapiou et al., 2020a)
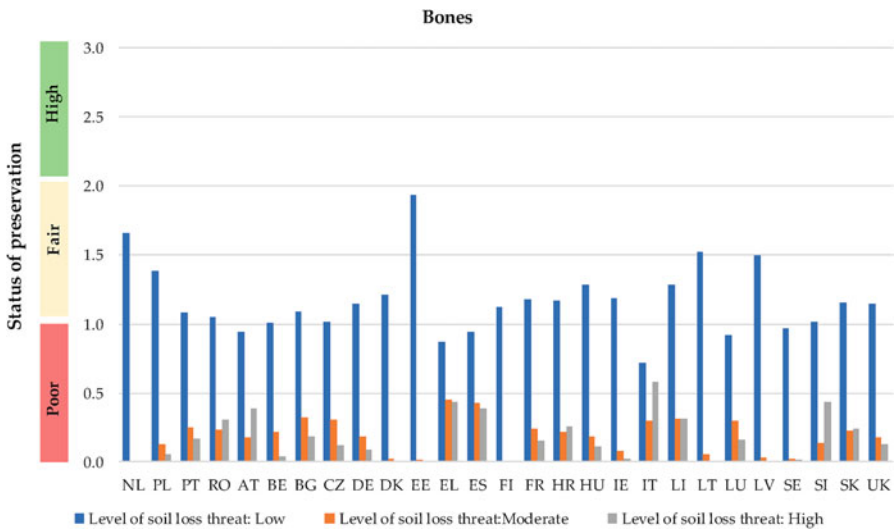

Fig. 8.6 Mean values per country level for bones per level of soil-loss threats: Values close to 1 indicate the poor preservation status, values close to 2 indicate fair conditions of preservation, and values close to 3 good preservation status. (Source: Agapiou et al., 2020a)

Fig. 8.7 Mean values per country level for organics per level of soil-loss threats: Values close to 1 indicate the poor preservation status, values close to 2 indicate fair conditions of preservation, and values close to 3 good preservation status. (Source: Agapiou et al., 2020a)
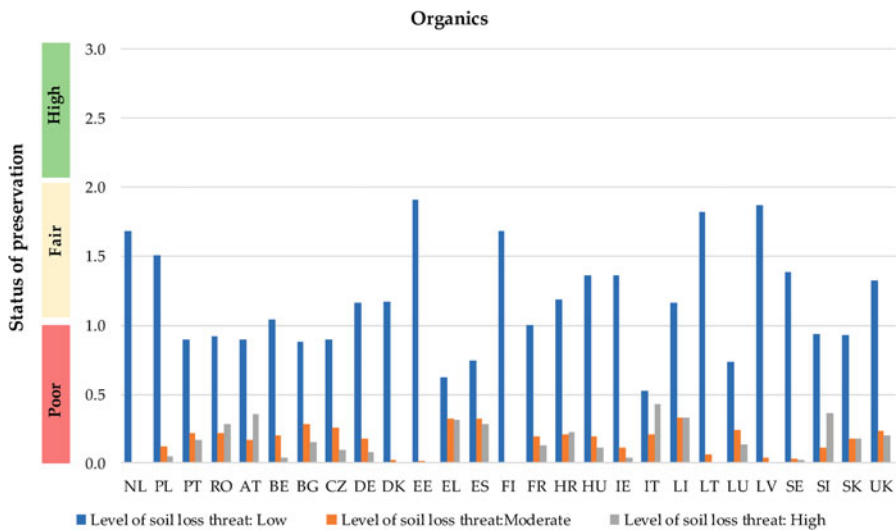

Fig. 8.8 Mean values per country level for bones per level of soil-loss threats: Values close to 1 indicate the poor preservation status, values close to 2 indicate fair conditions of preservation, and values close to 3 good preservation status. (Source: Agapiou et al., 2020a)
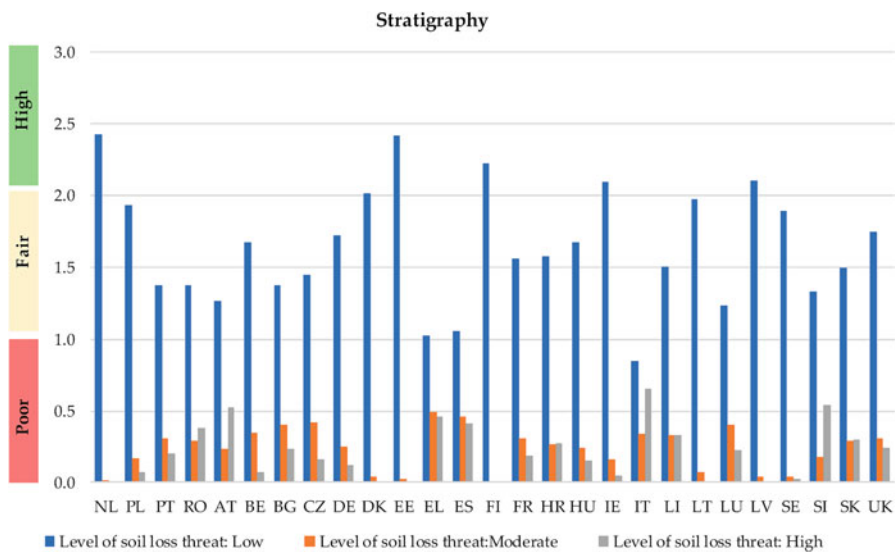
8.3.2   Vegetation Growth and Its Dynamics

Monitoring vegetation dynamics and long-term temporal changes of vegetation cover is of great importance for assessing the risk level of a natural or anthropogenic hazard. Vegetation plays a critical role in several hazards, like the soil loss mentioned earlier. The increase or decrease of vegetation cover through vegetation indices has been used in the past as an indicator for land-use change and urbanisation sprawl. At the same time, it can be an indication of agricultural pressure near archaeological sites' surroundings. The extraction of vegetation cover has been systematically investigated in the literature using optical satellite sensors. However, the use of radar vegetation indices is limited, while their combination is even rarer.

Several studies have demonstrated the benefits of satellite-based monitoring, providing comprehensive and systematic coverage over archaeological sites (Luo et al., 2019; Agapiou and Lysandrou, 2015). Open and freely distributed optical and radar satellite images are available from the European Copernicus Programme (2021). The Sentinel sensors, with a high-temporal revisit time, medium resolution satellite images can be downloaded through specialised big data cloud platforms such as the Sentinel Hub. At the same time, radiometric and geometric corrections can be applied.

To evaluate the overall performance of the synergistic use of optical and radar vegetation indices from the Sentinel-1 and Sentinel-2 sensors, Agapiou (2020) has used these datasets over the archaeological site of "Nea Paphos" in Cyprus. The study has also used other open access services, namely the crowdsourced OpenStreetMap initiative. In detail, optical and radar Sentinel datasets, acquired over the archaeological site of "Nea Paphos" have been used, while Sentinel ready products from the Sentinel Hub service and crowdsourced vector geodata available at the OpenStreetMap service have been explored. Finally, compressed red-green-blue (RGB) high-resolution optical data from the Google Earth platform for validation purposes were used (Fig. 8.9).

From the Sentinel Hub service, radar and optical Sentinel images were retrieved, and the Normalised Difference Vegetation Index (NDVI) and the Radar Vegetation Index (RVI) were processed using Eqs. 1 and 2:

$$NDVI = (\rho_{NIR} - \rho_{RED})/(\rho_{NIR} + \rho_{RED}), \qquad (8.1)$$

$$RVI = (VV/(VV + VH))^{0.5}\, (4\, VH)/(VV + VH), \qquad (8.2)$$

Where ρ_{NIR} and ρ_{RED} refer to the reflectance values (%) of the near-infrared and red bands of the optical Sentinel-2 sensor (band 8 and band 4), while the VV and VH refer to the polarisation bands of the Sentinel-1 sensor, implemented by a custom script available with the Sentinel-Hub services (2021).

Based on the optical and radar vegetation indices, the proportion of vegetation was then retrieved. In our study, two different models have been applied for both optical and radar datasets:
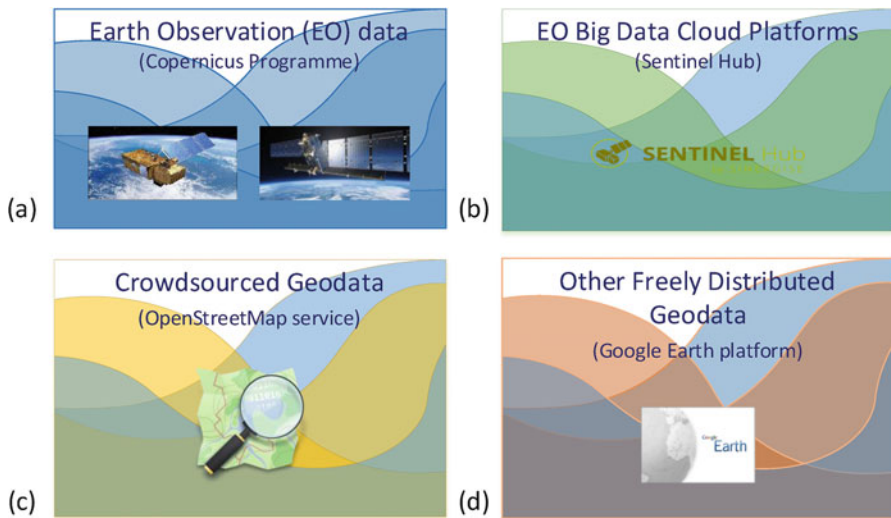
Fig. 8.9 A schematic representation of the four "layers" of information used the study of Agapiou (2020): the Earth Observation Sentinel-1 and Sentinel-2 images (top left), the Sentinel Hub, an Earth Observation big data cloud platform (top right), crowdsourced geodata from OpenStreetMap (bottom left) and the Google Earth platform (bottom right)

$$Pv_1 - radar = (RVI - RVI\ non - veg.)/(RVI\ veg - RVI\ non - veg.), \qquad (8.3)$$

$$Pv_1 - optical = (NDVI - NDVI\ non - veg.)/(NDVI\ veg - NDVI\ non - veg.), \qquad (8.4)$$

$$Pv_2 - radar = [(RVI - RVI\ min\,)/(RVI\ max\, - RVI\ min\,)]^{0.5} \qquad (8.5)$$

$$Pv_2 - optical = [(NDVI - NDVI\ min\,)/(NDVI\ max\, - NDVI\ min\,)]^{0.5} \qquad (8.6)$$

Where vegetation index veg (NDVI veg and RVI veg) and non-vegetation index (NDVI non-veg. and RVI non-veg.) represent the vegetated and non-vegetated pixels of the considered index, respectively, vegetation index max (NDVI max and RVI max) and vegetation index min (NDVI min and RVI min) represent the maximum and minimum histogram value of the vegetation image.

To investigate pottential correlation between the NDVI and the RVI indices, a regression analysis was carried out. As shown in Fig. 8.10, no specific pattern between the two indices can be extracted since there was a high variance. This is also aligned with the previous findings indicating that optical and radar indices do not produce similar findings.

In the light of the above, periodic monthly RVI and NDVI indices covering May 2019 to May 2020 were extracted from the Sentinel Hub service. RVI results over the "Nea Paphos" archaeological site are shown in Fig. 8.11-left, while Fig. 8.11-right shows the NDVI index results (whereas a – l in both figures refers to months starting from May 2019). Higher RVI values that could correspond to
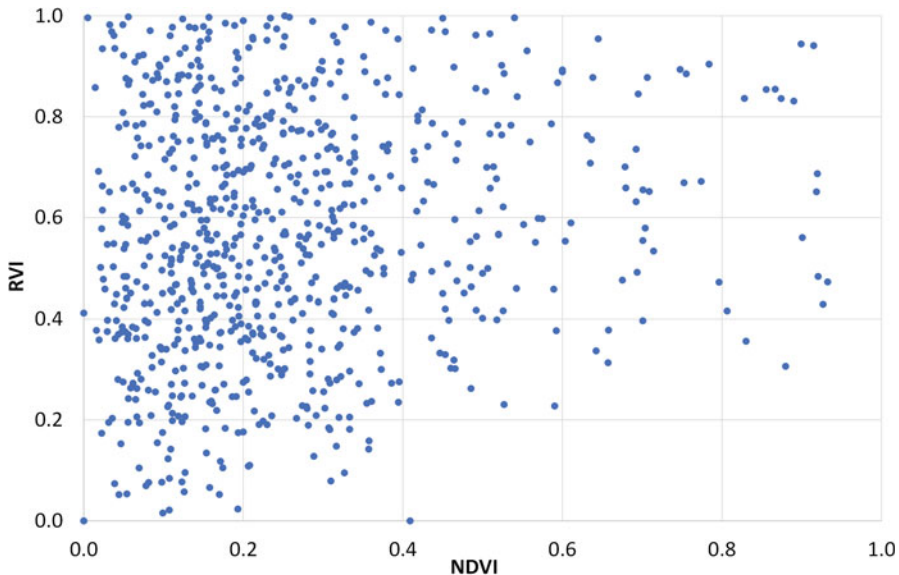
Fig. 8.10 Scatterplot of NDVI and RVI values over 1000 random points in the case study area
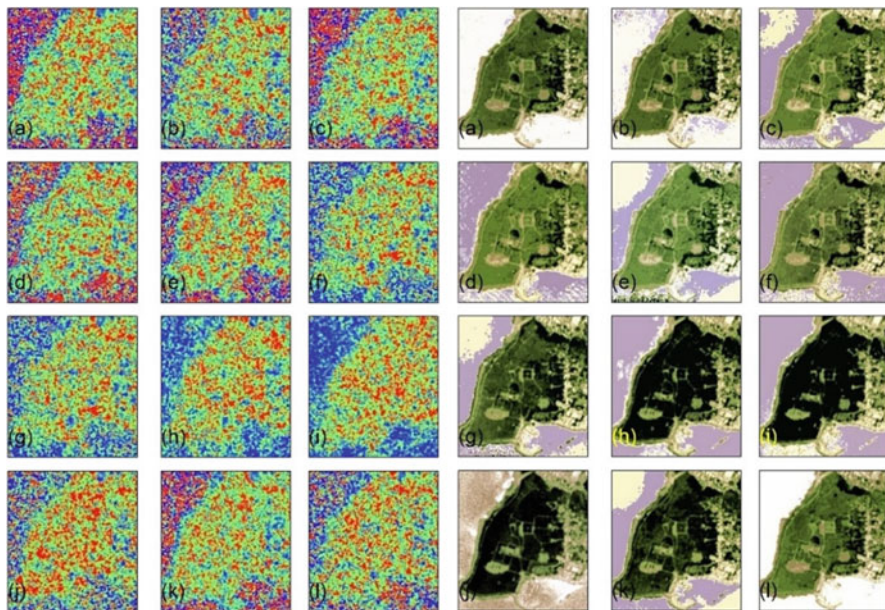
Fig. 8.11 Monthly RVI (left) and NDVI results (right) (**a**: May 2019, **b**: June 2019, **c**: July 2019, **d**: Aug. 2019, **e**: Sept. 2019, **f**: Oct. 2019, **g**: Nov. 2019, **h**: Dec. 2019, **i**: Jan. 2020, **j**: Feb. 2020, **k**: March 2020 and **l**: April 2020). (Source: Agapiou, 2020)

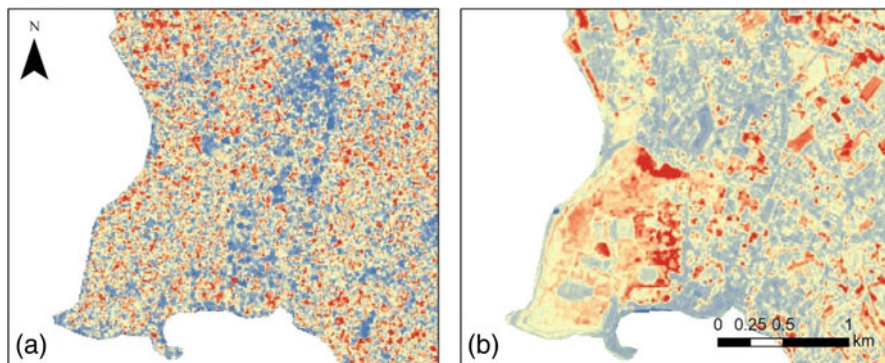**Fig. 8.12** (**a**) The difference in the proportion of vegetation cover as estimated from the RVI index is based on Eqs. 8.3 and 8.5 and (**b**) the difference in the proportion of vegetation cover as estimated from the NDVI index based on Eqs. 8.4 and 8.6. Higher difference values are indicated with red colour, while lower values with blue colour. (Source: Agapiou, 2020)

vegetation growth are highlighted with red colour in Fig. 8.11-left, while the dark green colour in Fig. 8.11-right shows vegetation at the optical products. The results show that Sentinel-2 images using the NDVI index can depict the vegetation's phenological changes over the "Nea Paphos" archaeological site throughout the year. In contrast, the interpretation of the RVI index is still problematic (Fig. 8.11-left). Nevertheless, an increase in vegetation (red colour) is evident during the months Dec. 2019 to Feb. 2020 (Fig. 8.11-left, h–j), which is also visible to optical products as well (Fig. 8.11-right, h–j).

Then, the vegetation proportion (see Eqs. 8.3, 8.4, 8.5, and 8.6) have been estimated for each type of sensors. These results were compared over the archaeological site of "Nea Paphos". Figure 8.12 a shows the difference between the OpenStreetMap (Eq. 8.3) and image statistics (Eq. 8.5) for the RVI index, while Fig. 8.12b the difference between the proportion of vegetation cover using the NDVI index (Eqs. 8.4 and 8.6). Higher differences are highlighted with red colour, while lower differences are estimated with blue colour.

The findings described above show that the NDVI and the RVI indices did not provide comparable results. Optical indices like the NDVI can be interpreted more easily in contrast to the RVI results. However, in some cases, such as the findings of Fig. 8.11, suggest that radar products can be used as an alternative to optical data for detecting patterns (e.g. vegetation growth) in specific areas of interest.

The study of Agapiou (2020) proposed a framework, whereas both proportions of vegetation indices derived from Sentinel-1 and -2 sensors can be used by multiplying the RVI x NDVI datasets. This outcome can be used with the VV and VH polarisations of Sentinel-1 to create a new pseudocolour composite. Radar datasets can depict urban areas, which can enhance the difference between vegetated and urban areas. An example of such a new composite is shown in Fig. 8.13. The NDVI proportion was estimated over the archaeological site of "Nea Paphos", using Sentinel-2 spectral bands 4 and 8. In contrast, the RVI vegetation proportion was
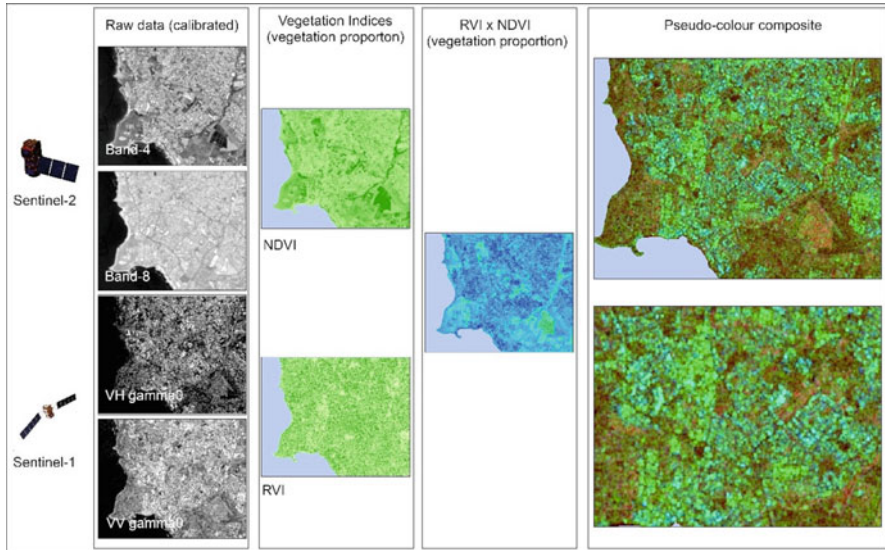
Fig. 8.13 New pseudo colour composite on the right-left of the Figure integrating the RVI x NDVI vegetation proportion index and the VV / VH polarisations from Sentinel 1. Vegetated areas are shown with red colour, while buildings with green colour. On the left side, the overall procedure (as explained in the previous sections) for estimating the RVI x NDVI index. (Source: Agapiou, 2020)

estimated using the VV and VH polarisations of the radar Sentinel-1. The combination of the two new products generates the new RVI x NDVI vegetation proportion index, which can be combined with the VV and the VH polarisations to highlight vegetated areas (see red colour areas under the pseudocolour composite of Fig. 8.13) and buildings (see with green colour areas under the pseudocolour composite of Fig. 8.13).

8.3.3 Surface Displacements

Earth observation may support the disaster risk management cycle, as this is understood for cultural heritage in multiple ways. At the same time, related technologies can change the traditional way of processing earth observation's data, specifically, from desktop analysis to cloud-based, for instance, the use of Google Earth Engine (GEE, 2021) for archaeological and heritage management studies (Orengo et al., 2020; Agapiou, 2017). This section presents an example of the Hybrid Pluggable Processing Pipeline (HyP3) cloud-based system, operated by the Alaska Satellite Facility (ASF), a related new cloud platform. To our knowledge, this

platform has not been hitherto used for heritage management (Agapiou & Lysandrou, 2020).

One of the most significant earthquakes that hit Cyprus in recent years was a 5.6 magnitude scale seismic event on 15th April 2015, at 08:25 UTC, and it was strongly felt throughout the country. The earthquake's epicenter was estimated at 8 km NW of Paphos (western Cyprus), with a depth of 27.62 km. This earthquake remains the biggest in Cyprus -until today- from the launch of the Sentinel-1 sensors in 2014.

In this study, two pairs of Sentinel-1 images were used in ascending (south pole towards the north pole) and descending orbit (north pole towards the south pole). For each pair, an image before and after the event was elaborated. InSAR deformation analysis was executed through the HyP3 platform. In particular, the InSAR GAMMA algorithm was used. The methodology describing the GAMMA software for InSAR analysis using Sentinel images comprises eleven (11) steps as described in Agapiou and Lysandrou (2020).

A vertical displacement map was generated from the HyP3 platform under the assumption that the interferometric phase is related solely to the topography of the area. Values were given in meters, with positive values indicating uplift and negative values indicating subsidence. The area of the earthquake's epicentre, the Paphos town, hosts significant archaeological sites and monuments, some of them listed as UNESCO World Heritage.

The InSAR analysis resulted in small ground displacements in this area, both from the images taken in ascending orbit and the seismic network. Figure 8.14a indicates the results from the unwrapped interferogram, while Fig. 8.14b shows the results from the vertical displacement analysis. Fig. 8.14c shows the coherence values based on the pair of Sentinel-1 images used in the ascending orbit. Areas with low coherence values (less than 70%, Fig. 8.14c) were excluded from the analysis.

A critical finding of that study was that the satellite datasets were processed in less than 1-hour for each orbit, significantly minimising the computational time compared to traditional desktop analysis. The use of ARD products produced from cloud-based platforms like the HyP3 is significant for heritage management. They can provide displacement information over large areas in a short time. However, as in almost all earth observation processing chains, these results require ground verifications from ground stations.

8.4   Risk Maps Using Various Hazards

As earlier stated, several hazards can affect archaeological assets, both individual monuments and entire sites. An Analytical Hierarchy Process (AHP) method, a multi-criteria decision-making method based on comparing concepts (alternatives) in pairs, can be implemented to address individual and unique characteristics of monuments and sites, creating small clusters. AHP is a straightforward approach,
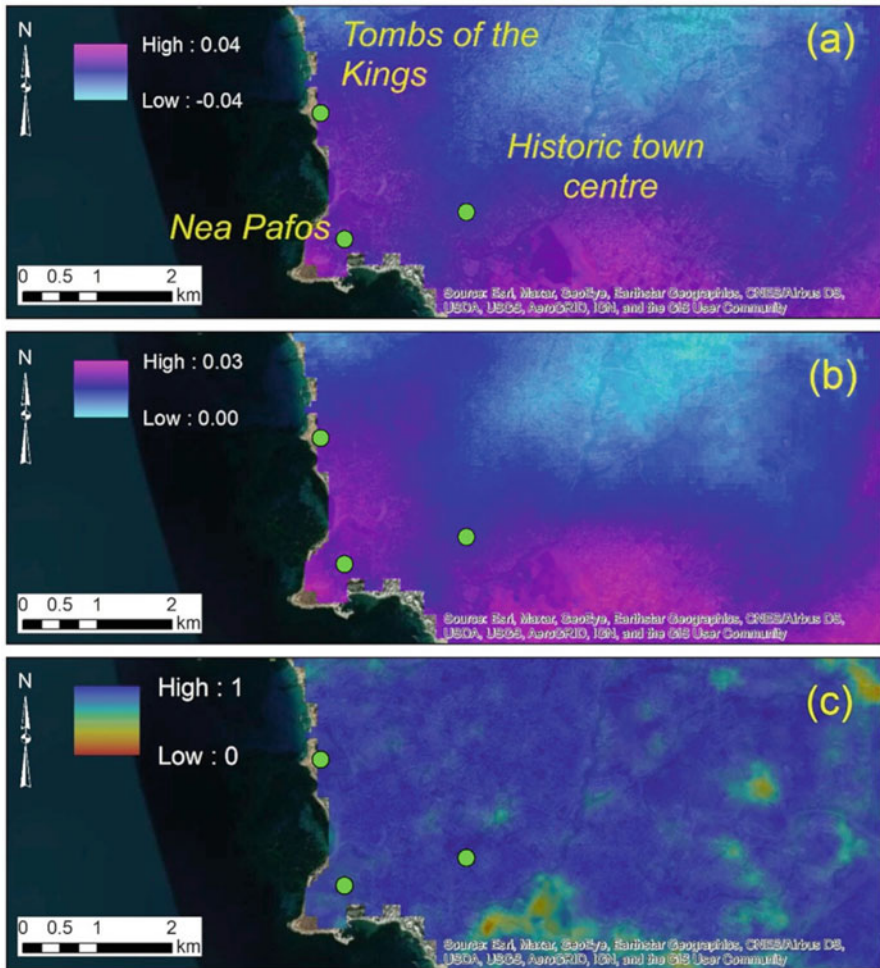
Fig. 8.14 (**a**) Unwrapped interferogram; (**b**) Vertical displacements; (c) Coherence map, enveloping archaeological sites of the area. (Source: Agapiou & Lysandrou, 2020)

widely applied to help decision-making mainly when several conflicting criteria are simultaneously occurring. Saaty (1977) has proposed AHP in the 1970s.

The study carried out by Agapiou et al. (2016b) was focused on the Paphos district in western Cyprus, an area that abounds in antiquities. More than 150 declared Ancient Monuments of First (Ancient Monuments on State Land) and Second Schedule (Ancient Monuments on Private Land) protected by the Antiquities Law had been mapped with high accuracy (Fig. 8.15). The authors have conducted previous research in this area to create a common geo-database of all monuments, estimating hazards, and produce risk maps from remote sensing data
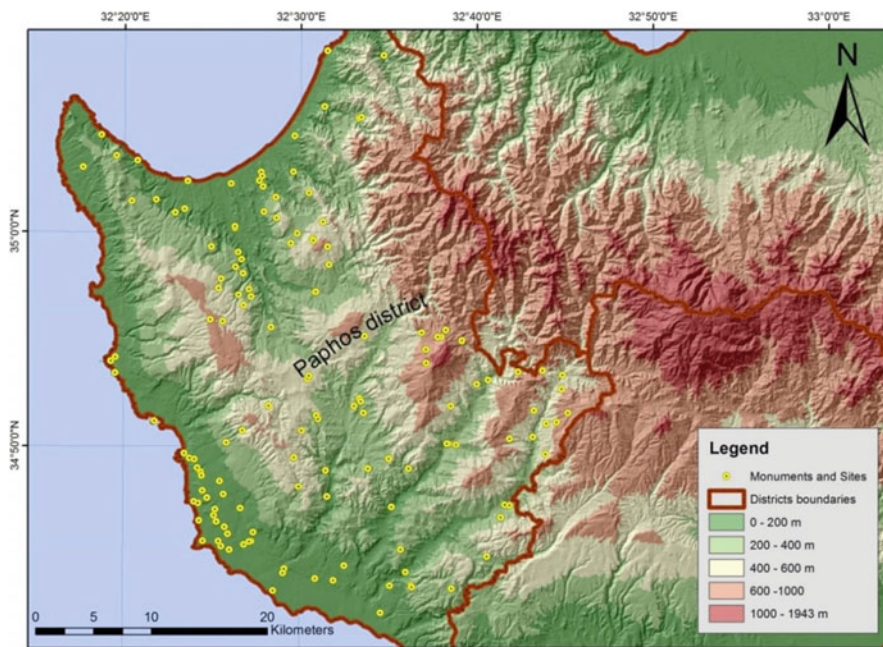
Fig. 8.15 Protected monuments and sites in Paphos district, Cyprus. (Source: Agapiou et al., 2016b)

(Agapiou et al., 2013). These monuments were clustered into five groups that shared similar geomorphological characteristics.

A variety of remote sensing datasets were used to map natural and anthropogenic hazards over this area. The list included low, medium and high-resolution satellite images like the MODIS, Landsat and QuickBird, along with ready satellite products, like the ASTER Global Digital Elevation Model, ASTER GDEM. Initially, each hazard was analysed. Then, the overall risk was estimated based on the AHP methodology. A series of risk maps were created relative to anthropogenic (urban sprawl, modern road network, fires) and environmental (erosion, salinity, neotectonic activity) hazards that affect the archaeological sites in the Paphos district. The resulting risk maps for each hazard are illustrated in Fig. 8.16 (for further information, see Agapiou et al., 2015).

For each one of the five different clusters, a separate AHP was implemented. Table 8.1 shows the weight factors for each group of monuments and each hazard. The highest weight for each class is highlighted in the table. The weights might vary significantly for each hazard, depending on the importance of each of the five classes. This difference of weights recorded for the same hazards in the different classes is normal since each group of monuments (class) faces dissimilar proportions since these are correlated to the site's location, amongst others.
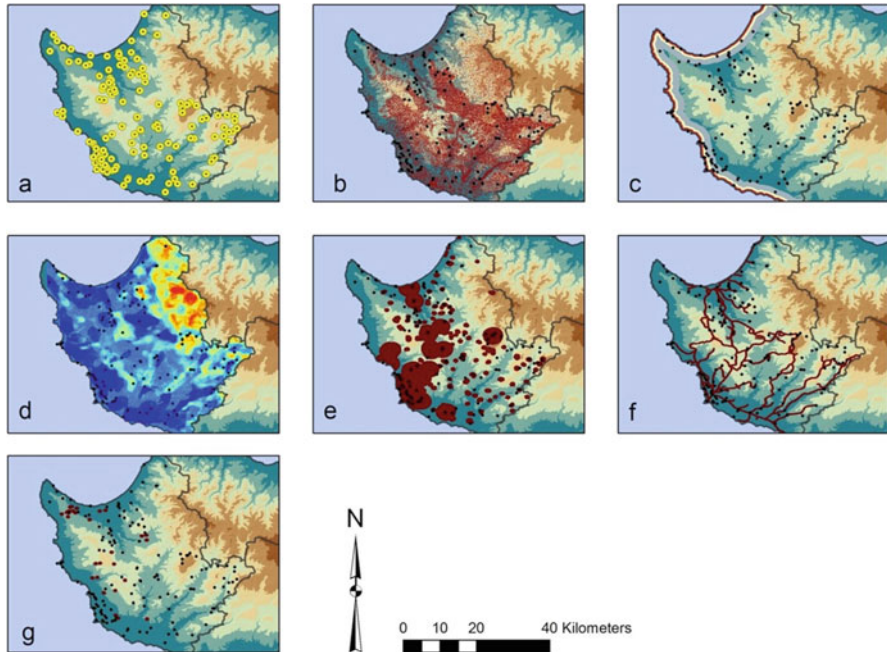
Fig. 8.16 Map indicating the different anthropogenic and natural hazards over the Paphos District. (**a**) Archaeological sites of the Paphos district; (**b**) Erosion map: areas, where the soil loss is greater than the mean value soil loss of the whole district, are indicated with red colour; (**c**) Salinity map: areas close to the sea are indicated with red; (**d**) Tectonic Activity: high and very high hazard area are indicated with red while the very low hazard is indicated with blue colour; (**e**) Urban expansion indicated with red colour; (**f**) Road network proximity (250 m) indicated with red colour which is linked with potential future urban expansion; and (**g**) Fires map observed during the period 2010-2013 indicated with red colour. (Revised map from Agapiou et al., 2015)

Using the weights shown in Table 8.1, the following equations for overall risk hazard for each group of monuments was estimated:

$$\text{Risk Hazard for Group 1} = 0.2500 * F1 + 0.0213 * F2 + 0.1302 * F3 \\ + 0.2747 * F4 + 0.0555 * F5 + 0.2683 * F6 \quad (8.7)$$

$$\text{Risk Hazard for Group 2} = 0.3928 * F1 + 0.0174 * F2 + 0.0679 * F3 \\ + 0.1209 * F4 + 0.1142 * F5 + 0.2868 * F6 \quad (8.8)$$

$$\text{Risk Hazard for Group 3} = 0.0906 * F1 + 0.0207 * F2 + 0.2061 * F3 \\ + 0.2390 * F4 + 0.1468 * F5 + 0.2968 * F6 \quad (8.9)$$

$$\text{Risk Hazard for Group 4} = 0.1436 * F1 + 0.1251 * F2 + 0.2339 * F3 \\ + 0.4114 * F4 + 0.0257 * F5 + 0.0603 * F6 \quad (8.10)$$

Table 8.1 AHP factors for the five different classes (groups) of monuments

	AHP weight factors for Group 1							
	Factors	F1	F2	F3	F4	F5	F6	Total Sum	Normalised Weights
1	Tectonic	1	1/9	5	3	9	3	21.11	0.2500
2	Salinity	1/9	1	1/7	1/9	1/3	1/9	1.800	0.0213
3	Road Network	1/3	7	1	1/3	3	1/3	11.00	0.1302
4	Urban areas	1/5	9	3	1	7	3	23.20	0.2747
5	Soil erosion	1/9	3	1/3	1/7	1	1/9	4.690	0.0555
6	Fires	1/3	9	3	1/3	9	1	22.66	0.2683
								84.46	**1**

	AHP weight factors for Group 2							
	Factors	F1	F2	F3	F4	F5	F6	Total Sum	Normalised Weights
1	Tectonic	1	9	9	9	7	5	40.00	0.3928
2	Salinity	1/9	1	1/5	1/5	1/7	1/9	1.77	0.0174
3	Road Network	1/9	5	1	1/3	1/3	1/7	6.92	0.0679
4	Urban areas	1/9	5	3	1	3	1/5	12.31	0.1209
5	Soil erosion	1/7	7	3	1/3	1	1/7	11.62	0.1142
6	Fires	1/5	9	7	5	7	1	29.20	0.2868
								101.82	**1**

	AHP weight factors for Group 3							
	Factors	F1	F2	F3	F4	F5	F6	Total Sum	Normalised Weights
1	Tectonic	1	5	1/3	1/3	1/3	1/3	7.33	0.0906
2	Salinity	1/5	1	1/9	1/9	1/7	1/9	1.67	0.0207
3	Road Network	3	9	1	1/3	3	1/3	16.67	0.2061
4	Urban areas	3	9	3	1	3	1/3	19.33	0.2390
5	Soil erosion	3	7	1/3	1/3	1	1/5	11.87	0.1468
6	Fires	3	9	3	3	5	1	24.00	0.2968
								80.87	**1**

	AHP weight factors for Group 4							
	Factors	F1	F2	F3	F4	F5	F6	Total Sum	Normalised Weights
1	Tectonic	1	1/3	1/3	1/5	7	3	11.87	0.1436
2	Salinity	3	1	1/5	1/7	3	3	10.34	0.1251
3	Road Network	3	5	1	1/3	5	5	19.33	0.2339
4	Urban areas	5	7	3	1	9	9	34.00	0.4114
5	Soil erosion	1/7	1/3	1/5	1/9	1	1/3	2.12	0.0257
6	Fires	1/3	1/3	1/5	1/9	3	1	4.98	0.0603
								82.64	**1**

	AHP weight factors for Group 5							
	Factors	F1	F2	F3	F4	F5	F6	Total Sum	Normalised Weights
1	Tectonic	1	9	7	3	3	9	32.00	0.3289
2	Salinity	1/9	1	1/7	1/9	1/5	1/5	1.76	0.0181
3	Road Network	1/7	7	1	1/3	3	3	14.47	0.1487
4	Urban areas	1/3	9	3	1	5	5	23.33	0.2398
5	Soil erosion	1/3	5	1/3	1/5	1	3	9.86	0.1014
6	Fires	9	5	1/3	1/5	1/3	1	15.86	0.1630
								97.28	**1**

Source: Agapiou et al. (2016b)

$$\text{Risk Hazard for Group 5} = 0.3289 * F1 + 0.0181 * F2 + 0.1487 * F3$$
$$+ 0.2398 * F4 + 0.1014 * F5 + 0.1630 * F6 \quad (8.11)$$

Where F1 to F6 stand for the different hazards (Tectonic; Salinity; Road Network; Urban areas; Soil erosion and Fires respectively), based on Table 8.1, the normalised weights for each risk have been added to the attribute table of the monuments in a GIS environment. Then, interpolation was carried out in a GIS environment, based on the Inverse Distance Weight (IDW) algorithm. The results from the interpolation of the weight factors are presented in Fig. 8.17. It should be noticed that in comparison with traditional AHP methodology, a single value would be allocated for all monuments in the Paphos district.

Then the overall risk hazard map was produced by multiplying the weight factor and the hazard:

$$\text{Overall Risk} = \text{Weight 1} * F1 + \text{Weight 2} * F2 + \text{Weight 3} * F3$$
$$+ \text{Weight 4} * F4 + \text{Weight 5} * F5 + \text{Weight 6} * F6 \quad (8.12)$$

Figure 8.18 shows the overall risk hazard map, where the five main categories are classified using natural breaks values. These categories are: (1) very low hazard, (2) low hazard; (3) medium hazard; (4) high hazard; (5) very high hazard. The areas under the indication of very high hazard, are located in Paphos town and immediate environs, where significant archaeological areas lie.

8.5 Conclusions

This chapter presented examples from earth observation studies related to the monitoring of archaeological/cultural heritage sites over Cyprus. The chapter was based on published work, a result of recent research, while it also delivered new concepts and applications using cloud-based earth observation platforms.

Section 3.1 reports the threat of subsurface archaeological remains from soil erosion, exploiting existing geo-data. The results showed that although most of the archaeological sites are characterised as "low threat" areas, significant differences between regions (north and south Europe) can be seen. Section 3.2 focused on the caption of vegetation dynamics using integrated optical and radar sensors. Vegetation is a critical factor for several hazards like urbanisation and soil loss. A pseudocolour composite was retrieved over urban and vegetated areas by applying the NDVI and the RVI indices. Further studies are needed in this direction. Moreover, InSAR analysis through the HyP3 platform has been presented.

Estimation of threats over extensive areas, like the case study of Paphos District, was carried out using the AHP methodology. More than 150 monuments of this area were grouped into five classes based on specific characteristics. The overall risk was
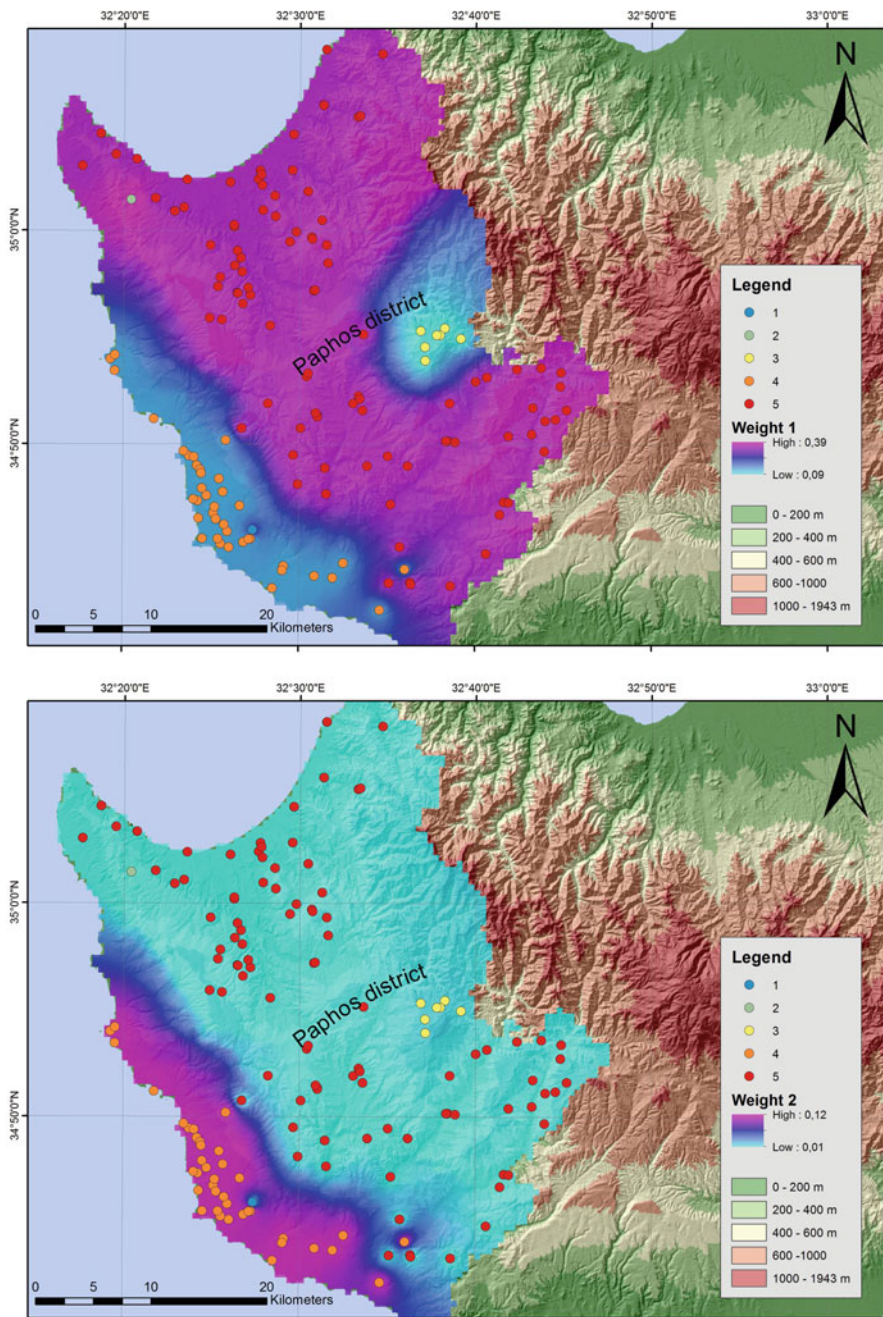
Fig. 8.17 Interpolation of the different normalisation weight for each hazard (Weight 1 to 6: Tectonic; Salinity; Road Network; Urban areas; Soil erosion and Fires respectively). (Source: Agapiou et al., 2016b)
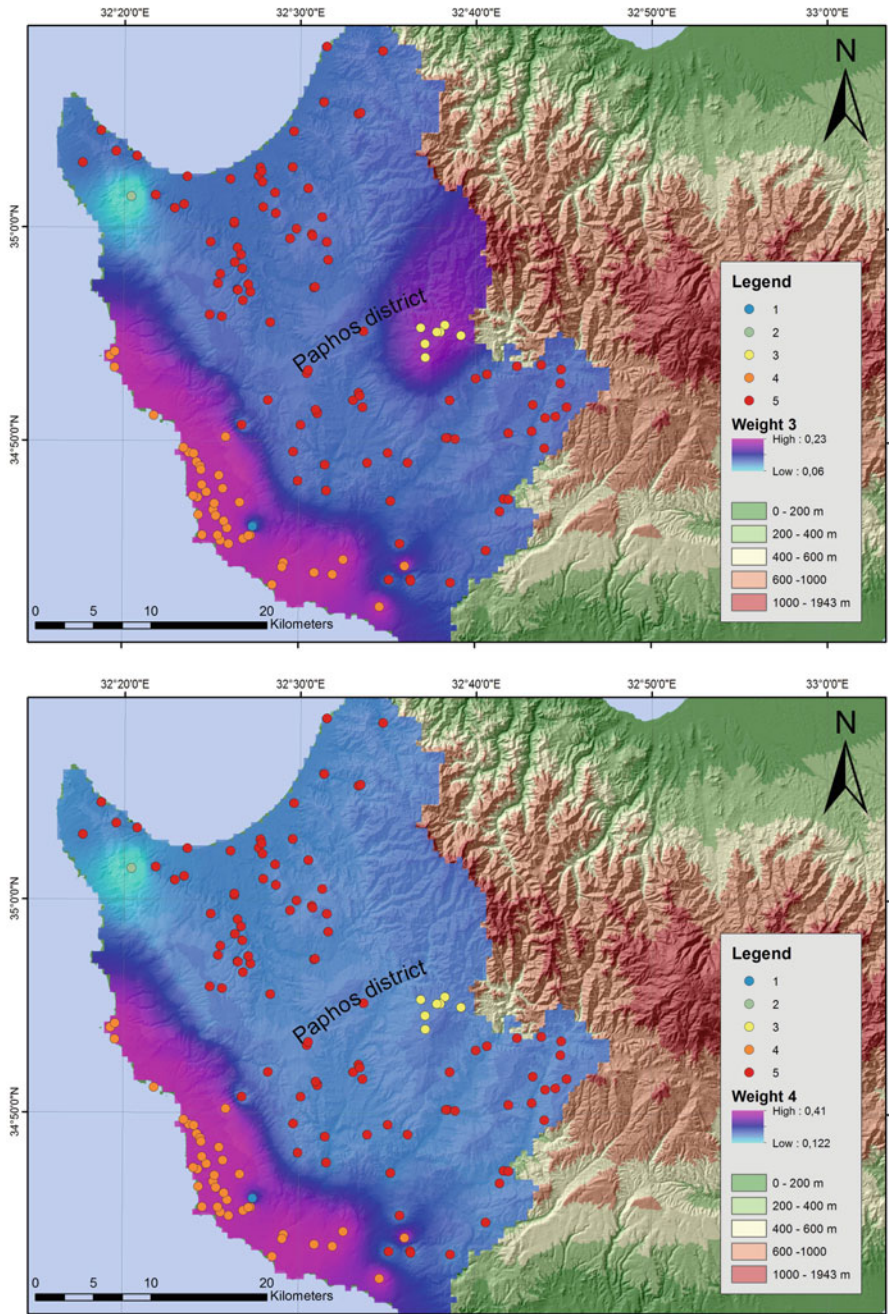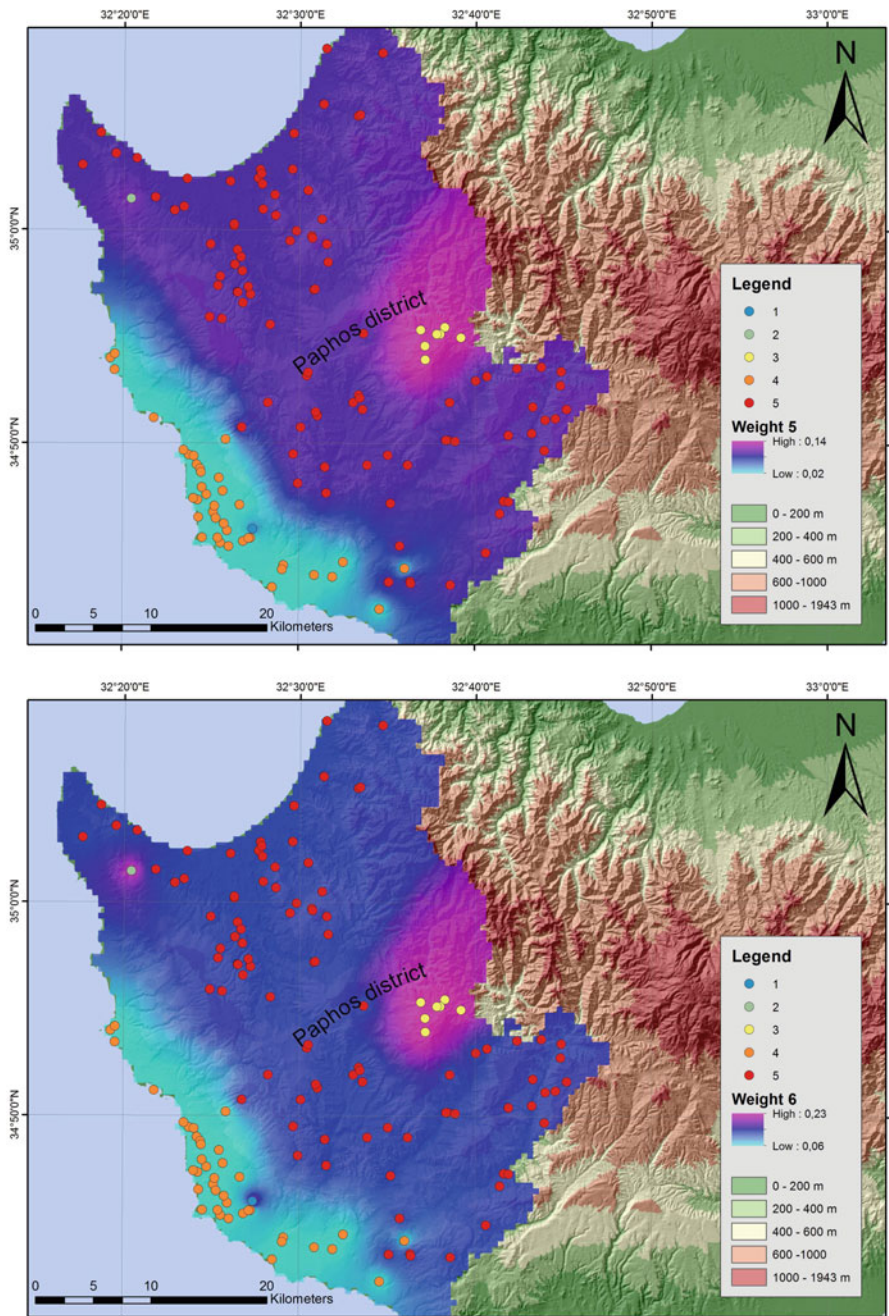
Fig. 8.17 (continued)
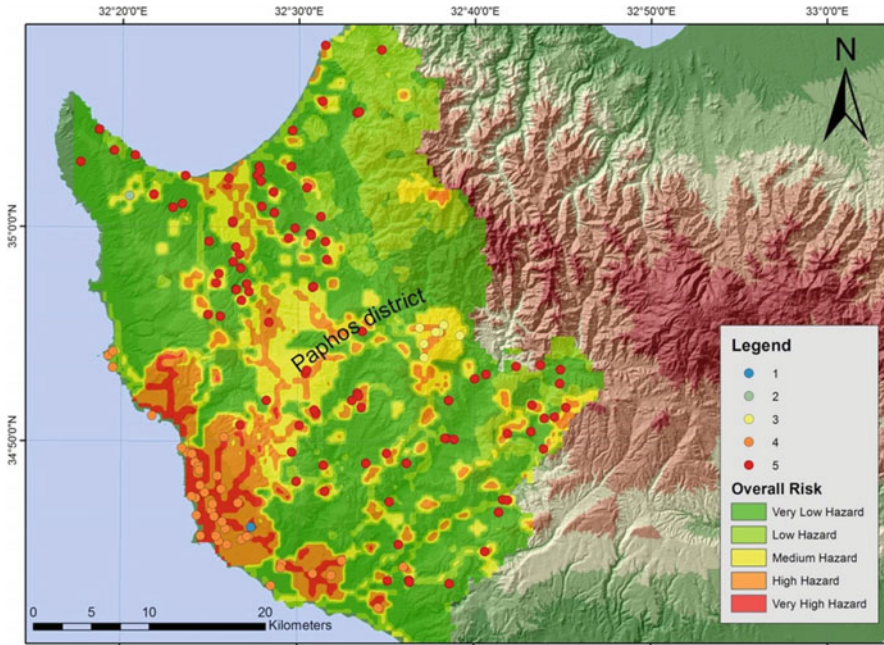
Fig. 8.17 (continued)

Fig. 8.18 Overall risk hazard map for the Paphos district, based on the clustering of the sites. (Source: Agapiou et al., 2016b)

estimated for each group, and afterwards, the overall risk prioritisation was carried out.

A key to the quality assurance of the applications above, methodologies and tools, is multidisciplinary collaboration. Future trends in the domain of earth observation indicate that technological changes will affect how space-based monitoring and observation are performed. This will be primarily based on cloud-platforms while the use of ready products will become more frequently used by the end-users and local stakeholders.

References

Abarquez, I., & Murshed, Z. (2004). *Field practitioners' handbook, community-based disaster risk management*. Asian Disaster Preparedness Centre.

Agapiou, A. (2017). Remote sensing heritage in a petabyte-scale: Satellite data and heritage earth Engine© applications. *International Journal of Digital Earth, 10*, 85–102.

Agapiou, A. (2020). Estimating proportion of vegetation cover at the vicinity of archaeological sites using Sentinel-1 and -2 data, supplemented by Crowdsourced OpenStreet Map Geodata. *Applied Sciences, 10*, 4764. https://doi.org/10.3390/app10144764

Agapiou, A., & Lysandrou, V. (2015). Remote Sensing Archaeology: Tracking and mapping evolution in scientific literature from 1999–2015. *Journal of Archaeological Science: Reports, 4*, 192–200.

Agapiou, A., & Lysandrou, V. (2020). Detecting displacements within archaeological sites in Cyprus after a 5.6 magnitude scale earthquake event through the Hybrid Pluggable Processing Pipeline (HyP3) cloud-based system and Sentinel-1 Interferometric Synthetic Aperture Radar (InSAR) Analysis. *IEEE Journal of Selected Topics in Applied Earth Observations and Remote Sensing, 13*, 6115–6123. https://doi.org/10.1109/JSTARS.2020.3028272

Agapiou, A., Nisantzi, A., Lysandrou, V., Mammouri, R., Alexakis, D. D., Themistocleous, K., Sarris, A., & Hadjimitsis, D. G. (2013). Mapping air pollution using earth observation techniques for cultural heritage. Proceedings SPIE 8795. *First International Conference on Remote Sensing and Geoinformation of the Environment (RSCy2013) 87950K.* https://doi.org/10.1117/12.2028234.

Agapiou, A., Lysandrou, V., Alexakis, D. D., Themistocleous, K., Cuca, B., Sarris, A., Argyrou, N., & Hadjimitsis, D. G. (2015). Cultural heritage management and monitoring using remote sensing data and GIS: the case study of Paphos area, Cyprus. *CEUS Computers Environment and Urban Systems, 54*, 230–239. https://doi.org/10.1016/j.compenvurbsys.2015.09.003

Agapiou, A., Alexakis, D. D., Sarris, A., & Hadjimitsis, D. G. (2016a). Colour to greyscale pixels: re-seeing greyscale archived aerial photographs and declassified satellite CORONA images based on image fusion techniques. *Archaeological Prospection, 23*, 231–241. https://doi.org/10.1002/arp.1536

Agapiou, A., Lysandrou, V., Themistocleous, K., et al. (2016b). Risk assessment of cultural heritage sites clusters using satellite imagery and GIS: the case study of Paphos District, Cyprus. *Natural Hazards, 83*, 5–20. https://doi.org/10.1007/s11069-016-2211-6

Agapiou, A., Lysandrou, V., & Hadjimitsis, D. G. (2020a). A European-scale investigation of soil erosion threat to subsurface archaeological remains. *Remote Sensing, 12*, 675. https://doi.org/10.3390/rs12040675

Agapiou, A., Lysandrou, V., & Hadjimitsis, D. G. (2020b). Earth observation contribution to cultural heritage disaster risk management: Case study of Eastern Mediterranean open air archaeological monuments and sites. *Remote Sensing, 12*, 1330. https://doi.org/10.3390/rs12081330

Borrelli, P., Robinson, D. A., & Fleischer, L. R. (2013). An assessment of the global impact of 21st century land use change on soil erosion. *Nature Communications, 8*. https://doi.org/10.1038/s41467-017-02142-7

Bosco, C., de Rigo, D., Dewitte, O., Poesen, J. (2021). *Copernicus emergency management services.* https://emergency.copernicus.eu. Accessed on 22 Feb 2021.

Casana, J. (2020). Global-scale archaeological prospection using CORONA satellite imagery: Automated, crowd-sourced, and expert-led approaches. *Journal of Field Archaeology, 45*(Suppl 1), S89–S100. https://doi.org/10.1080/00934690.2020.1713285

Chandramohan, T., Venkatesh, B., & Balchand, A. N. (2015). Evaluation of three soil erosion models for small watersheds. *Aquatic Procedia, 4*, 1227–1234. https://doi.org/10.1016/j.aqpro.2015.02.156

Emergency Management Australia. (2000). *Emergency risk management – Applications guide* (Australian emergency manuals series). www.ema.gov.au

Erosion by Water, Joint Research Centre European Soil Data Centre (ESDAC). (2021). Available online: https://esdac.jrc.ec.europa.eu/themes/erosion. Accessed on 22 Feb 2021.

European Copernicus Programme. (2021). https://www.copernicus.eu/en. Accessed on 22 Feb 2021.

Ghosal, K., & Das Bhattacharya, S. (2020). A Review of RUSLE Model. *Journal of the Indian Society of Remote Sensing*. https://doi.org/10.1007/s12524-019-01097-0

Google Earth Engine (GEE). (2021). https://earthengine.google.com. Accessed on 22 Feb 2021.

Group on Earth Observations (GEO). (2021). https://www.earthobservations.org/geoss_wp.php. Accessed on 22 Feb 2021.

Hritz, C. (2013). A malarial-ridden swamp: using Google Earth Pro and Corona to access the southern Balikh valley, Syria. *Journal of Archaeological Science, 40*(4), 1975–1987.

ICCROM. (2016). *A Guide to Risk Management of Cultural Heritage 2016*. Government of Canada, Canadian Conservation Institute.

International Charter Space and Major Disasters. (2021). https://disasterscharter.org/web/guest/home;jsessionid=25223736C25BDBEEF6EBF9BC7CA46695.jvm1.   Accessed   on 22 Feb 2021.

ISO 31000. (2018). *Risk management – Guidelines*. https://www.iso.org/standard/65694.html. Accessed on 22 Feb 2021.

Kibblewhite, M., Tóth, G., & Hermann, T. (2015). Predicting the preservation of cultural artefacts and buried materials in soil. *Science of the Total Environment, 529*, 249–263.

Li, J., & Roy, D. P. (2017). A global analysis of Sentinel-2A, Sentinel-2B and Landsat-8 data revisit intervals and implications for terrestrial monitoring. *Remote Sensing, 9*, 902.

Luo, L., Wang, X., Guo, H., Lasaponara, R., Zong, X., Masini, N., Wang, G., Shi, P., Khatteli, H., Chen, F., et al. (2019). Airborne and spaceborne remote sensing for archaeological and cultural heritage applications: A review of the century (1907–2017). *Remote Sensing of Environment, 232*, 111280.

Lysandrou, V., & Agapiou, A. (2020). The role of archival aerial photography in shaping our understanding of the Funerary Landscape of Hellenistic and Roman Cyprus. *Open Archaeology, 6*(1), 417–433. https://doi.org/10.1515/opar-2020-0117

Orengo, A. H., Conesa, C. F., Garcia-Molsosa, A., Lobo, A., Green, A. S., Madella, M., & Petrie, C. A. (2020). Automated detection of archaeological mounds using machine-learning classification of multisensory and multitemporal satellite data. *Proceedings of the National Academy of Sciences Aug, 117*(31), 18240–18250. https://doi.org/10.1073/pnas.2005583117

Panagos, P. (2015). Modelling soil erosion at European scale: Towards harmonisation and reproducibility. *Natural Hazards and Earth System Sciences, 15*, 225–245. https://doi.org/10.5194/nhess-15-225-2015

Panagos, P., & Katsoyiannis, A. (2019). Soil erosion modelling: The new challenges as the result of policy developments in Europe. *Environmental Research, 172*, 470–474. https://doi.org/10.1016/j.envres.2019.02.043

Panagos, P., Van Liedekerke, M., Jones, A., & Montanarella, L. (2012). European Soil Data Centre: Response to European policy support and public data requirements. *Land Use Policy, 29*(2), 329–338. https://doi.org/10.1016/j.landusepol.2011.07.003

Pastonchi, L., Barra, A., Monserrat, O., Luzi, G., Solari, L., & Tofani, V. (2018). Satellite data to improve the knowledge of geohazards in world heritage sites. *Remote Sensing, 10*, 992.

Pena, B. S., Abreu, M. M., Magalhães, R. M., & Cortez, N. (2020). Water erosion aspects of land degradation neutrality to landscape planning tools at national scale. *Geoderma, 363*, 114093. https://doi.org/10.1016/j.geoderma.2019.114093

Quinton, J. N. (2011). Soil Erosion Modeling. In J. Gliński, J. Horabik, & J. Lipiec (Eds.), *Encyclopedia of agrophysics; encyclopedia of earth sciences series*. Springer.

Renard, K. G., Foster, G. R., Weesies, G. A., McCool, D. K., & Yoder, D. C. (1997). *Predicting soil erosion by water: A guide to conservation planning with the Revised Universal Soil Loss Equation (RUSLE)*. US Department of Agriculture, Agricultural Research Service.

Saaty, T. L. (1977). A scaling method for priorities in hierarchical structures. *Journal of Mathematical Psychology, 15*(3), 234–281.

Sentinel-Hub services, custom scripts. (2021). https://custom-scripts.sentinel-hub.com/sentinel-1/radar_vegetation_index. Accessed on 22 Feb 2021.

Solari, L., Bianchini, S., Franceschini, R., Barra, A., Monserrat, O., Thuegaz, P., Bertolo, D., Crosetto, M., & Catani, F. (2020). Satellite interferometric data for landslide intensity evaluation in mountainous regions. *International Journal of Applied Earth Observation and Geoinformation, 87*.

Tapete, D., Cigna, F., & Donoghue, N. M. D. (2016). Looting marks' in space-borne SAR imagery: Measuring rates of archaeological looting in Apamea (Syria) with TerraSAR-X staring spotlight. *Remote Sensing of Environment, 178*, 42–58.

UNESCO (Paris), et al. (2010). *Managing disaster risks for world heritage. World heritage resource manual* (p. 69). United nations educational, scientific and cultural organisation (UNESCO).

United Nations. (2009). *UNISDR terminology on disaster risk reduction* (p. 35). United Nations International Strategy for Disaster Reduction (UNISDR) 2009.

United Nations Platform for Space-based Information for Disaster Management and Emergency Response (UN-SPIDER). (2021). https://www.unoosa.org/oosa/en/ourwork/un-spider/index. html. Accessed on 22 Feb 2021.

Ur, J. A. (2016). Middle Eastern archaeology from the air and space. *In Situ Fall*, 1–4.